How do the Local Physical, Biochemical, and Mechanical Properties of an Injectable Synthetic Anisotropic Hydrogel Affect Oriented Nerve Growth?

Susan Babu, I Chen, Sitara Vedaraman, José Gerardo-Nava, Christopher Licht, Yonca Kittel, Tamás Haraszti, Jacopo Di Russo, and Laura De Laporte*

As an injectable tissue regenerative platform, Anisogel aims to recapitulate the complex and anisotropic architecture of native extracellular matrix by the use of magneto-responsive microgels, which are oriented under a low magnetic field of ≈100 mT, while a surrounding hydrogel matrix cross-links around them. This system promotes the oriented growth of neurons when cultured in vitro. In this study, how the local microgel properties affect neurite outgrowth and orientation is aimed to understand using dorsal root ganglia from chicken embryos. When the surrounding matrix is a synthetic poly(ethylene glycol) hydrogel, the microgel concentration and length required to achieve oriented nerve growth is higher compared to fibrin-based Anisogels. Microgels should be stiffer than the matrix for cells to sense the mechanical anisotropy but a wide range of microgel stiffness leads to similar cell alignment and growth. On the other hand, modification of the microgels with common extracellular matrix molecules enhances nerve growth but deteriorates nerve alignment compared to bioinert microgels in a cell adhesive surrounding gel. Finally, covalently coupling these microgels to the surrounding matrix reduces both cellular orientation and outgrowth suggesting a reduction in the ability of cells to sense the anisotropy.

1. Introduction

Tissue engineering for therapeutic applications is a rapidly growing field of research, with the aim to restore, maintain, or enhance the tissue and organ function by providing more accessible and safer alternative to the conventional tissue or organ transplantation procedures from donors.[1] Few organs in the adult mammalian bodies have an innate ability to regenerate, while others can do so with the introduction of various types of exogenous progenitor cells or stem cells.[2] In case of the several tissues with limited regenerative capacities, such as those of heart, central nervous system, pancreas, and kidney, more complex strategies to direct regeneration are required, utilizing novel biomaterials that can provide mechanical support, structural integrity and various biochemical and biophysical cues to the damaged tissue.[3–5] Among the different classes of biomaterials available today, hydrogels are the most popular ones used for this purpose, owing to their similarities with the native extracellular matrix (ECM) in both structure and composition.

Over the years, many different types of hydrogels have been used for tissue regeneration, which are of either synthetic or natural origin, or a combination there of, and have different chemical building blocks and cross-linking mechanisms.[6,7] Recently, several efforts have been made to

S. Babu, I Chen, S. Vedaraman, J. Gerardo-Nava, C. Licht, Y. Kittel,
T. Haraszti, J. Di Russo, L. De Laporte
DWI – Leibniz Institute for Interactive Materials
Forckenbeckstrasse 50, 52074 Aachen, Germany
E-mail: delaporte@dwi.rwth-aachen.de

S. Babu, I Chen, L. De Laporte
Max Planck School – Matter to Life (MtL)
Jahnstraße 29, 69120 Heidelberg, Germany

S. Babu, S. Vedaraman, Y. Kittel, T. Haraszti, L. De Laporte
Institute of Technical and Macromolecular Chemistry (ITMC)
Polymeric Biomaterials
RWTH University Aachen
Worringerweg 2, 52074 Aachen, Germany

J. Di Russo
Interdisciplinary Centre for Clinical Research
RWTH Aachen University
Aachen, Germany

J. Di Russo
Institute of Molecular and Cellular Anatomy
RWTH Aachen University
Wendlingweg 2, 52057 Aachen, Germany

L. De Laporte
Advanced Materials for Biomedicine (AMB)
Institute of Applied Medical Engineering (AME)
University Hospital RWTH Aachen
Center for Biohybrid Medical Systems (CMBS)
Forckenbeckstrasse 55, 52074 Aachen, Germany

ADVANCED
SCIENCE NEWS
www.advancedsciencenews.com

ADVANCED
FUNCTIONAL
MATERIALS
www.afm-journal.de

create multiscale structures in these hydrogels for the regeneration of aligned tissues by means of electrospinning, stretching, directional freeze drying, etc.,[8–11] with electrospinning being the most widely used technique to introduce structural anisotropy. Electrospun fibres have been utilized to produce aligned implantable scaffolds either by themselves or in combination with other hydrogel materials to direct nerve regeneration.[12–14] (3D) bioprinting is yet another innovative technique to incorporate heterogeneity in structures that can be shaped to perfectly fit the injury site.[15,16] A scalable and facile method to produce aligned bioprinted hydrogels utilizing elongated microgels were realized by passing pre-cross-linked bulk hydrogels through a perforated grid to form entangled microstrands. These microstrands either contain cells or can be mixed with cells after extrusion. Myoblasts cultured in such a system were found to form aligned myotubes after differentiation.[17] One downside of the above methods is that the resulted scaffolds require surgical interventions for implantation, which may cause further tissue damage. In this context, hydrogels that can be delivered by injection into the injured site are of particular interest in the regeneration of sensitive tissues, providing a minimally invasive method. These hydrogels could be directly administered to the lesion site without the requirement of a surgery and would very rapidly undergo gelation under the physiological conditions of the body.[7,18,19] Although these hydrogels hold great potential in the field of regenerative therapy, conventional hydrogels suffer from a major drawback of being isotropic, meaning they possess a homogenous structure, with that it is difficult to mimic and thereafter regenerate more complex, hierarchically organized oriented tissues, such as heart, muscle or spinal cord.[9] A solution to this is the use of injectable anisotropic hydrogels for tissues that are too sensitive to recover from any damage caused during an invasive surgery.

The most recent advances in the development of injectable and heterogeneous hydrogels for tissue regeneration have been extensively discussed in our recently published review article.[19] To introduce anisotropy in 3D hydrogels, photopatterning using a focused laser beam to form regions of higher stiffness was recently found to induce cell alignment in the regions outside of the irradiated regions.[21] Although suitable in vitro, a limited depth of light penetration hampers the use of this method in vivo. Another method to introduce aligned domains in injectable hydrogels involves the use of self-assembling peptides to form aligned nanofibrils upon injection under physiological conditions. These peptides could be modified to present cell adhesive peptides like IKVAV to promote neuronal growth and alignment.[22,23] Recently, it was shown that such a system could be further engineered to present specific bioactive domains, such as a peptide that mimics fibroblast growth factor 2 (YRSRKYSSWYVALKR), which activates the fibroblast growth factor 2 receptor for promoting endothelial cell growth and angiogenesis, in addition to IKVAV. Besides these biological modifications, the mechanical properties of the resulting hydrogel were optimized to enable a significant functional recovery from a severe spinal cord injury in mouse.[24] In the latter study, the nanofibrils were not aligned using the flow-induced orientation, as mentioned in the previous studies, but the supramolecular species in these nanofibrils could undergo molecular motions in a nanometer scale. The plasticity of such

scaffolds and the molecular mobility of peptides were shown to enhance neurite growth, angiogenesis and enabled a functional recovery after spinal cord injury. Alternatively, magnetic alignment is a promising strategy to obtain anisotropic scaffolds. This is made possible by orienting the diamagnetic polymer fibrils of collagen or fibrin using a strong magnetic field (9.4 T)[25,26] or by the magnetic alignment and/or the self-assembly of diamagnetic cellulose nanocrystals[27,28] or superparamagnetic iron oxide nanoparticles (SPIONs)[29,30] in a hydrogel precursor solution under a magnetic field after injection. However, in both of these systems, the dimensional and mechanical control of aligned domains are limited. Besides, the latter one relies on the aggregation of SPIONs, which may cause cytotoxic issues when used in vivo, especially with the high concentration of SPIONs required.[31]

Lastly, a novel tissue regenerative platform called Anisogel, was introduced by our research group. Anisogels are comprised of magnetically oriented rod-shaped microgels or short fibres inside a surrounding hydrogel matrix (**Figure 1**). These microgels and fibres are rendered magneto-responsive by the incorporation of low concentrations of SPIONs (400 µg mL^{-1}) into them. When a hydrogel precursor solution containing these micro-elements is injected in the presence of a magnetic field (100 mT), the anisometric elements align along the direction of applied magnetic field, while the surrounding degradable hydrogel cross-links to fix this orientation. This prevents any further movement of the aligned elements even after the magnetic field is removed. During the entire duration of cell culture, the nanometre scale degradation of the hydrogel by cells does not reduce the microgels' orientation. Anisogels were shown to be successful in inducing fibroblasts and neurons to grow parallel to the direction of alignment when used in vitro.[32,33]

In the initial works done on Anisogels, a natural fibrin hydrogel was used as a matrix and it was shown that microgels of dimensions $5 \times 5 \times 50$ µm at a concentration of 1 vol% is sufficient to enable an oriented growth of dorsal root ganglion (DRG) neurons derived from chicken embryos.[32] Since these microgels possess a high aspect ratio, only a low concentration of SPIONs (400 µg mL^{-1}) is sufficient to prompt magnetic rotation and thus alignment of the microgels. As 1 vol% of these microgels are adequate in the final gel, the overall concentration of SPIONs was further reduced to just 4 µg mL^{-1}. Short fibres used in place of these microgels also produced a similar effect. The microgels are prepared by an in-mould polymerization technique using polyethylene glycol diacrylate (PEG-DA), whereas the fibres are made from poly(lactide-co-glycolide) (PLGA) or polycaprolactone via electrospinning or solvent-assisted spinning followed by micro-cutting.[34,35] While PLGA fibres are known to allow cell attachment without further biomodification through their hydrophobicity and rough surface,[36] they release acidic products over time and cause a drop in pH due to hydrolytic degradation.[37,38] In contrast, no such cell adhesion is possible on bioinert PEG microgels, while no harmful degradation products are obtained from them.[39] Owing to their bioinertness, we could conclude that the alignment of cells in Anisogels containing oriented microgels was caused by the different mechanical cues sensed by cells in the direction of alignment as opposed to the direction perpendicular to it. It could be shown that an increase in microgel

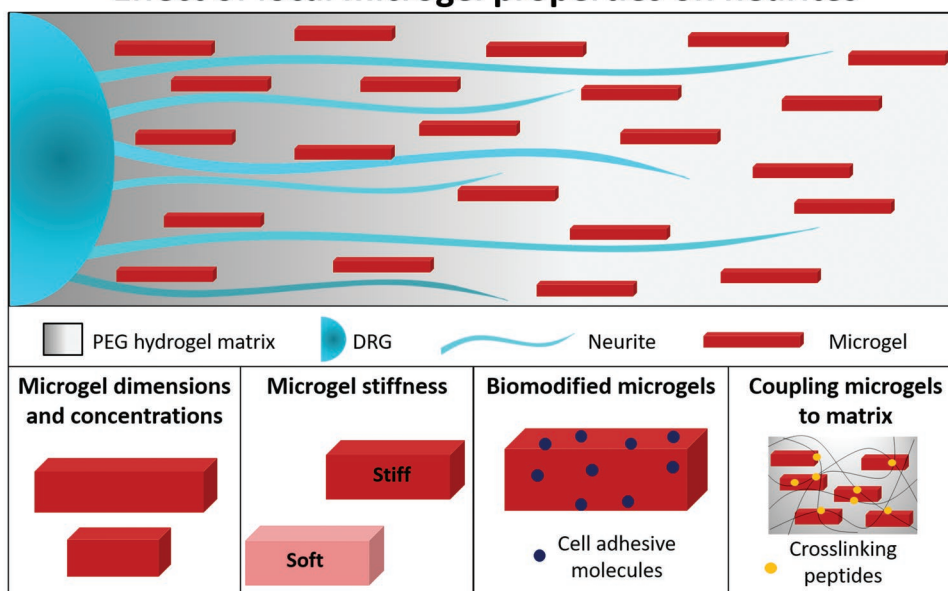## Effect of local microgel properties on neurites

Figure 1. A schematic of the Anisogel system with neurites growing aligned in the direction of microgels along with the local microgel properties that are modified to affect neuronal growth.

concentration in fibrin matrices enhanced nuclear YES-associated protein (YAP) shuttling in fibroblasts.[40] YAP is an important facilitator in the cellular mechanotransduction process[41,42] and its nuclear shuttling from the cytoplasm is an indicator of cells sensing the enhanced anisotropy introduced by the increased presence of microgels.[40] Moreover, microgels offer a wide range of variation in their physical, mechanical, and biochemical properties.

Following RGD modification on the microgels, cells exhibited a decreased secretion of ECM components like fibronectin compared to inert microgels. This is important as we found that the secreted ECM molecules in the case of inert microgel is also aligned,[40] which suggests a possible positive-feedback mechanism whereby cells can secrete their own oriented ECM to guide them further while the microgels would degrade away. Additionally, it was shown that microgels biomodified with GRGDS did not cause any significant improvement in nerve growth or alignment compared to the unmodified ones in fibrin-based Anisogels. These results indicate that over-stimulating cells may be detrimental to the positive feedback mechanism when an already bioactive surrounding matrix like fibrin is used for the growth of neurites. In the same Anisogel system, it was also observed that reducing the microgel thickness 5–2.5 µm enhances neurite growth while maintaining their alignment. Moreover, this was made possible at a much lower microgel concentration of 0.45 vol% inside the entire Anisogel.[43] This led to the understanding that thicker cross section of microgels can pose a barrier for the neurites to extend themselves efficiently in the Anisogels.

Since using fibrin as a surrounding matrix is not ideal for in vivo applications due to its fast degradation, a synthetic fibrin mimetic PEG-based hydrogel is currently used instead as the matrix for Anisogels.[35,44] It has already been shown that fully synthetic PEG-based Anisogels also enable an oriented growth of neurites. Besides this, a synthetic hydrogel allows to adjust the matrix properties like stiffness, degradation rate, and concentration of bioadhesive molecules independently to achieve the best conditions for nerve regeneration. However, it needs to be noted that these are mostly the bulk material properties of hydrogels, similar to many previous studies.[44–46] It is often challenging in such systems to look into the combinatorial effect of multiple local and global cues on cell growth, similar to the scenario in the native ECM. The effect of local hydrogel properties on cells in 3D hydrogel systems was explained in an earlier work using collagen gels prepared by the polymerization of collagen I at different temperatures.[47] Even though the collagen concentration was kept constant, the different polymerization temperatures gave rise to a range of fibre diameters and resultant stiffness. It was shown that stiffer and more bundled fibres led to improved cell adhesion stability, while more flexible and finer fibre networks enabled easier adhesion retractions. In case of Anisogels, the presence of the aligned magnetic microgels in a 3D hydrogel provides us with an invaluable tool to understand the role of orthogonal signals in promoting unidirectional growth of neurites in Anisogels.

In this paper, we employ the PEG-based Anisogel system to study how the local Anisogel properties affect neuronal growth and guidance. For this, we rely on microgels and their specific physical, mechanical, and biochemical properties to understand how important the local biomechanical cues are in dictating cell fate. We have used microgels of varying aspect ratios, volume percentages, stiffness, and surface biomodifications to achieve a better understanding of how these local changes in Anisogels, in addition to the already existing mechanical anisotropy, are affecting the cell responses.

**ADVANCED
SCIENCE NEWS**
www.advancedsciencenews.com

**ADVANCED
FUNCTIONAL
MATERIALS**
www.afm-journal.de

2. Results and Discussion

2.1. Comparison of Different Microgel Dimensions and Concentrations

In our previously published work on the PEG-based Anisogel system, it was observed that 5 × 5 × 50 µm sized aligned and bioinert PEG microgels at 1 vol% concentration, resulted in a reduced nerve alignment[35] in comparison to our fibrin-based Anisogel system, when similar dimensions and vol% of microgels were employed.[32] We hypothesize that the higher degree of nerve orientation in the fibrin-based Anisogel system is because the fibrin gels are inherently fibrous[26] and may be partly oriented during the formation of the Anisogel. However, for in vivo application, fibrin gels degrade too quickly and a PEG-based fibrin mimetic hydrogel was developed to achieve degradation on cell demand in a controlled manner.[35,46,48,49] Therefore, we here investigate how the anisotropy in PEG-based hydrogels can be improved and felt by the cells, by varying several design parameters. First, the dimensions and concentration of bioinert PEG microgels are varied. Based on our previous study demonstrating enhanced nerve extension in the case of thin microgels (2.5 × 2.5 × 25 µm), the thickness of microgels used in this study is fixed at 2.5 µm.[43] Two microgel lengths of 25 and 50 µm are used to compare different aspect ratios. The 2.5 × 2.5 × 25 µm sized microgels are used at 0.45 and 1 vol% concentrations, whereas the 2.5 × 2.5 × 50 µm sized microgels are tested at 0.6 and 1 vol% concentrations in the overall Anisogel. These concentrations are chosen to directly compare the alignment of neurites between the PEG-based Anisogel studied here and the previously published fibrin-based Anisogel system (Table 1).[43] The 2.5 × 2.5 × 25 µm sized microgels at 0.45 vol%, which is the optimal condition for fibrin-based Anisogels are compared with 0.6 vol% of 2.5 × 2.5 × 50 µm sized microgels to keep the inter-microgel distance constant at 24 µm. The 1 vol% concentrations of the two types of microgels are chosen to see the effect of a higher vol% for both microgel dimensions. The number of microgels per µL of the Anisogel and the inter-microgel distance are calculated as described previously.[43]

The PEG microgels are prepared using a technique called particle replication in non-wetting templates (PRINT). This is a soft-lithography technique that utilizes a soft elastomeric mould to form soft microgels with precise dimensions in the micrometer scale.[32,50] In this study, a polymer precursor solution is employed, consisting of 20 wt.% PEG-DA (700 Da), SPIONs (400 µg mL^{-1}), photoinitiator and a fluorescent dye in liquid PEG-OH (200 Da), which acts as a diluent to enable complete mould filling and prevents evaporation during the cross-linking process.[32] The non-reactive diluent is washed away during subsequent harvesting and purification steps. The mould cavities filled with the precursor solution are then cross-linked under UV-light in a nitrogen atmosphere. The microgels are harvested, purified, and sterilized as previously reported before their use in Anisogels.[32,40]

The PEG precursor molecules to form the surrounding PEG matrix of the fully synthetic Anisogels are prepared and stored in advance by coupling two peptides to 8 arm star PEG-vinylsulfone (sPEG-VS, 20 kDa) via Michael-type addition. One peptide possesses a transglutaminase substrate (H-NQEQVSPLERCG-NH2: Q-peptide) and a thiol-containing cysteine, while the second peptide consists of a free primary amine (Ac-FKGGG-PQGIWGQERCG-NH2: K-peptide), a cysteine, and a matrix metalloprotease (MMP) degradable sequence GPQIWGQ that enable cell-induced degradation to provide space for cells to grow inside the matrix. Before injection, these PEG-peptide conjugates are mixed with a buffer and other biological domains, after that they undergo an enzymatically-induced cross-linking reaction with each other by the addition of activated transglutaminase Factor XIII (FXIIIa) at a concentration of 50 U mL^{-1} to form a hydrogel after injection. A 1 w/v% of polymer concentration is used to yield a hydrogel with a storage modulus of the order 10 Pa as confirmed by rheological measurements (Figure S1, Supporting Information). It has been shown previously that only at this order of stiffness, these PEG gels support neurite growth and enable the highest level of fibroblast growth and spreading.[35] The gel also contains fibronectin (1 µm) as a bioactive protein to render the otherwise inert PEG gel cell adhesive. Owing to the high molecular weight of fibronectin (440 kDa), these molecules remain physically entangled in the PEG hydrogel without significantly changing the mechanical properties of the gel.[35] When preparing Anisogel samples, the cell culture media in the precursor solution contains a calculated number of microgels of specific dimensions to achieve a desired final concentration in the whole Anisogel. These samples are made by pipeting a small volume of the precursor solution into a suitable chamber fitted with magnets to provide a magnetic field of strength ≈100 mT. A dorsal root ganglion (DRG), extracted from a 10 days old chicken embryo, is carefully placed inside this solution before final cross-linking of the Anisogel to encapsulate the DRG inside the gel. DRGs are cultured for seven days, followed by fixation, staining for b-tubulin and imaging using a confocal microscope. The Anisogel images are analyzed for the orientation of neurites and the length of their outgrowth from the core. We consider the neurites oriented only if the full width half maximum (FWHM) of their orientation distribution curve falls below 90°.

Based on the images and graphs in **Figure 2**, it is clear that the PEG-based Anisogels are able to induce oriented neurite growth only with the 2.5 × 2.5 × 50 µm sized microgels at 1 vol% concentration, resulting in a mean FWHM of 87 ± 29° to represent the level of neurite alignment. This is significantly lower than the FWHM (127°) obtained with 1 vol% of 5 × 5 × 50 µm sized microgels in PEG-based Anisogels reported in the previous publication.[35] The 2.5 × 2.5 × 25 µm sized microgels of aspect ratio 10, which is sufficient to orient neurites in fibrin-based Anisogel system at 0.45 vol%,[43] failed to produce a similar effect in the PEG-based Anisogel system,

Table 1. The List of Different Microgel Dimensions and Concentrations Used in the Study.

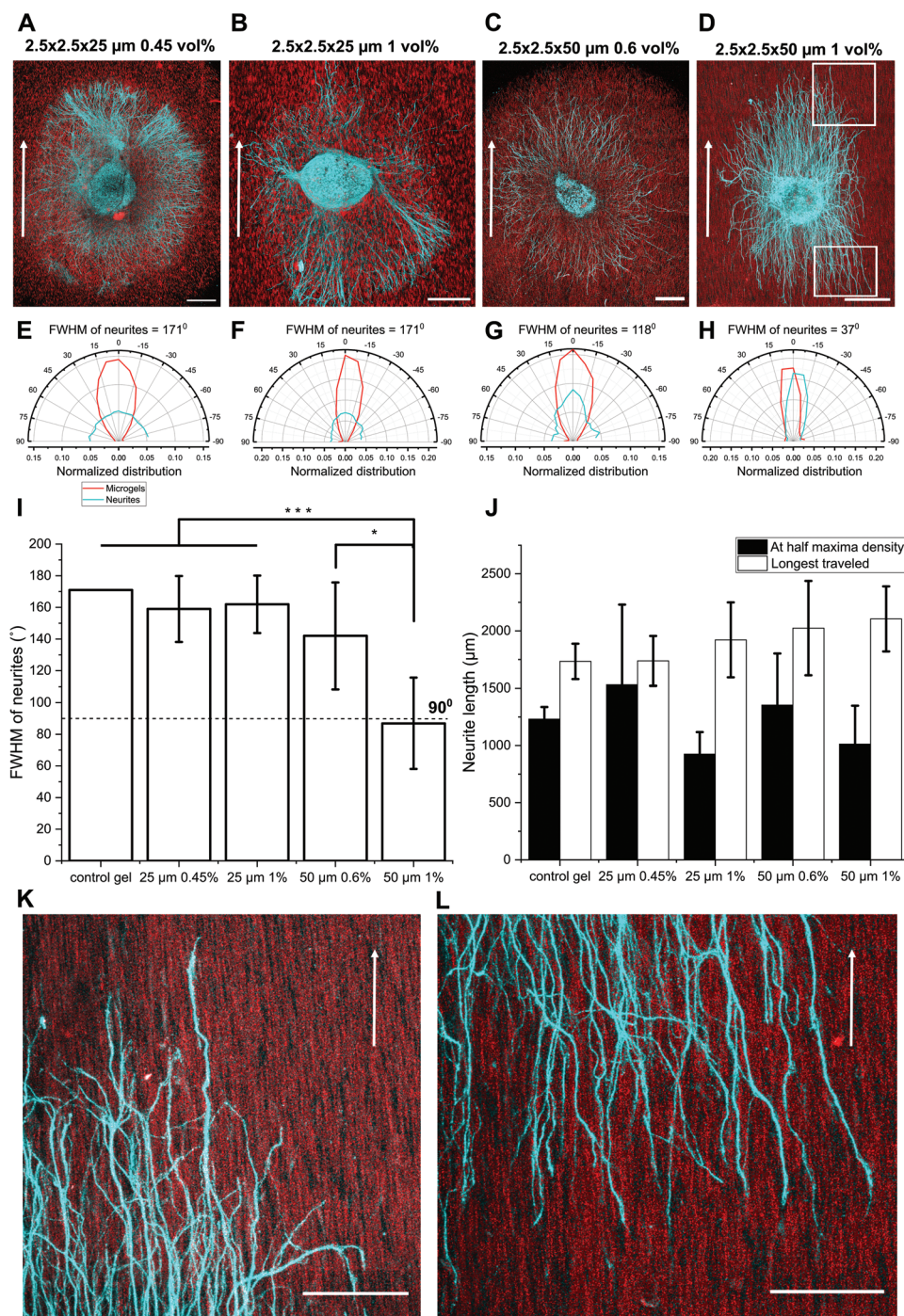| Diameter [µm]	Length [µm]	No. of microgels per µL	Volume %	Inter-microgel distance [µm]
2.5	25	29 061	0.45	24.0
2.5	25	64 000	1.00	16.8
2.5	50	19 243	0.60	24.0
2.5	50	32 000	1.00	18.8

Figure 2. Comparison of neurite orientation and growth in Anisogels having microgels of different dimensions and volume concentrations. A–D) Confocal micrographs of DRGs after seven days of culture in Anisogels containing aligned $2.5 \times 2.5 \times 25$ µm microgels at 0.45 vol%, $2.5 \times 2.5 \times 25$ µm microgels at 1 vol%, $2.5 \times 2.5 \times 50$ µm microgels at 0.6 vol%, and $2.5 \times 2.5 \times 50$ µm microgels at 1 vol% respectively. Cyan is *b*-tubulin and red is rhodamine-labeled microgels. Scale bar = 500 µm. $n \geq 3$ in all conditions. E–H) Representative orientation distribution curves of neurites and microgels in the respective Anisogel conditions. I) Plot comparing the FWHM of neurite orientation in different microgel conditions. Only those conditions with FWHM less than 90° are considered as aligned. J) Plot comparing the lengths at half maxima density of neurites and the longest distance travelled by neurites in different microgel conditions. Data is presented as mean ± s.d. and statistical significance was performed using one-way ANOVA with Tukey comparison (* $p < 0.05$; ** $p < 0.01$; *** $p < 0.001$). K,L) Magnified images of neurites growing in the Anisogel containing $2.5 \times 2.5 \times 50$ µm sized microgels at 1 vol%. The magnified regions are taken from image D from the highlighted regions marked by the white boxes. Scale bar = 200 µm. The white arrows indicate the direction of alignment of microgels.

resulting in a FWHM of 160 ± 21°, clearly indicating the requirement of additional directional guidance in the PEG gels. This might be due to the presence of a fibrillar network structure in fibrin gels, in contrast to the non-fibrous homogenous networks in PEG gels.[26] Increasing the concentration of these microgels to 1 vol% to reduce the inter-microgel distance from 34 to 17 µm, however, does also not cause any improvement in neurite orientation. On the other hand, increasing the microgel length to 50 µm, and thus the aspect ratio to 20, at a concentration of 0.6 vol% reduced the FWHM to 142 ± 34°. It is only when the concentration of these higher aspect ratio microgels was enhanced to 1 vol%, does the FWHM drops below our 90° threshold. For this condition, the mean inter-microgel distance is about 19 µm and the neurites are able to grow in a unidirectional manner, defined by thin aligned microgels. The combination of a lower inter-microgel distance with a smaller microgel thickness is thus more efficient than 1 vol% of 5 × 5 × 50 µm sized microgels, where the inter-microgel distance was about 34 µm. The extend of neurite outgrowth is quantified by two parameters, length at half maxima density of neurites and longest distance travelled by the neurites from the edge of the DRG core as described before.[44] For all conditions tested in this report using microgels with a width of 2.5 µm, no significant differences in neurite outgrowth are observed, even when compared with the control samples without any microgels. A representative image of the neurites grown in a control gel without microgels, along with its orientation distribution is shown in Figure S2 (Supporting Information). This proves that at all these concentrations, neurite outgrowth is not hindered by the presence of thin microgels.

2.2. Comparison of Different Microgel Stiffness

It is a well-established fact by now that 2D substrate stiffness at a fixed ligand density directly affects and controls the morphology and behavior of various adherent cell types. Soft elastic substrates give rise to reduced cell spreading and increased cell migration rates in association with highly dynamic and irregularly shaped focal adhesions.[51,52] Studies on cell durotaxis have also demonstrated that cells tend to migrate toward stiffer regions on a substrate exhibiting a stiffness gradient, with this behavior being more pronounced in the lower stiffness regime (2–7 kPa).[53] In a 3D environment, the situation is reversed with the stiffer matrices reducing cell spreading due to the increased resistance for cells to deform and remodel their environments.[54,55] In the context of PEG hydrogels used as the Anisogel matrix, it has already been understood that only the softest gel of storage modulus of the order 10 Pa can support neurite growth, in agreement with the above findings.[35] However, in a 3D Anisogel, cells can sense the anisotropy introduced by microgels with a stiffness that is significantly higher than that of their surrounding matrix. The currently known mechanisms of cell-matrix interactions in a 3D environment cannot fully explain the effect of these aligned stiff microgels in causing oriented cell growth, especially since these microgels are bioinert and do not provide any cell attachment sites for an integrin mediated guided cell migration. We previously observed that the cells do not require contact with the microgels

to grow parallel to their alignment.[40] When stained for the mechanosensitive protein YAP, an increase in its nuclear translocation was observed when the number of microgels were increased, independent of whether the cells were in contact with a microgel or not.[40] This suggests that the cells can sense the overall mechanical anisotropy from a certain distance away from the microgels. To see if we can further utilize this ability of cells to enhance their oriented growth in PEG-based Anisogels, we studied the effect of local microgel stiffness on neurite orientation and growth in a soft surrounding matrix.

Since these microgels are produced via free radical polymerization, there is a limitation in the lowest stiffness possible to obtain stable microgels.[56,57] Nevertheless, we altered the reactive polymer content PEG-DA in the precursor solutions 10–80 wt.% to produce microgels with a stiffness ranging 35–950 kPa measured by AFM point force spectroscopy (**Figure** 3K). The SPION concentration is maintained at 400 µg mL^{-1} and all Anisogel samples are prepared in the same manner as described in section 2.1. From the above-mentioned results, we have set the microgel dimensions and concentration to be 2.5 × 2.5 × 50 µm and 1 vol% in all further Anisogel conditions.

The results in Figure 3 clearly shows alignment of neurites in all five conditions with a FWHM ranging 56°–90°, compared to a FWHM of 161 ± 28° for the control condition without any microgels (Figure S2, Supporting Information). Surprisingly, there is, however, no statistically significant difference in FWHM that can be concluded from the graph between the different microgel stiffness conditions. All the microgels are thus equally capable of orienting the neurites inside the Anisogels. A similar observation is found in the neurite outgrowth analysis with no significant differences in neurite length among all conditions, including the control (Figure 3M). Even though a rise in local stiffness is imposed by increasing stiffness of the microgels, affecting the overall mechanical anisotropy of the Anisogel, neurite growth and alignment are not affected. This is likely due to the low hindrance for neurites to grow in the soft surrounding hydrogel matrix with thin microgels. The results suggest that the stiffness range we have used is still above the physiologically relevant range at which cells are more sensitive to local stiffness changes in order to display a difference in their behavior.[53] On the other hand, these results do prove that Anisogels can effectively promote cellular guidance with the use of relatively soft microgels, but with a stiffness sufficiently higher than the surrounding matrix. This is interesting for in vivo applications as the polymer concentration of the microgels will also affect their rate of degradation, thus offering a range of residence times inside the Anisogel, which may need to be altered depending on the regenerating tissue.

2.3. Effect of Microgel Biochemical Modification

Besides the substrate rigidity, the presence of bioactive molecules on hydrogel surfaces and in 3D matrices promotes cell spreading and proliferation.[44,58] Cells can adhere to various ECM proteins through their transmembrane receptors called integrins, which can link to the actin filaments in cells via focal adhesions.[59] These actin filaments further link dynamically to
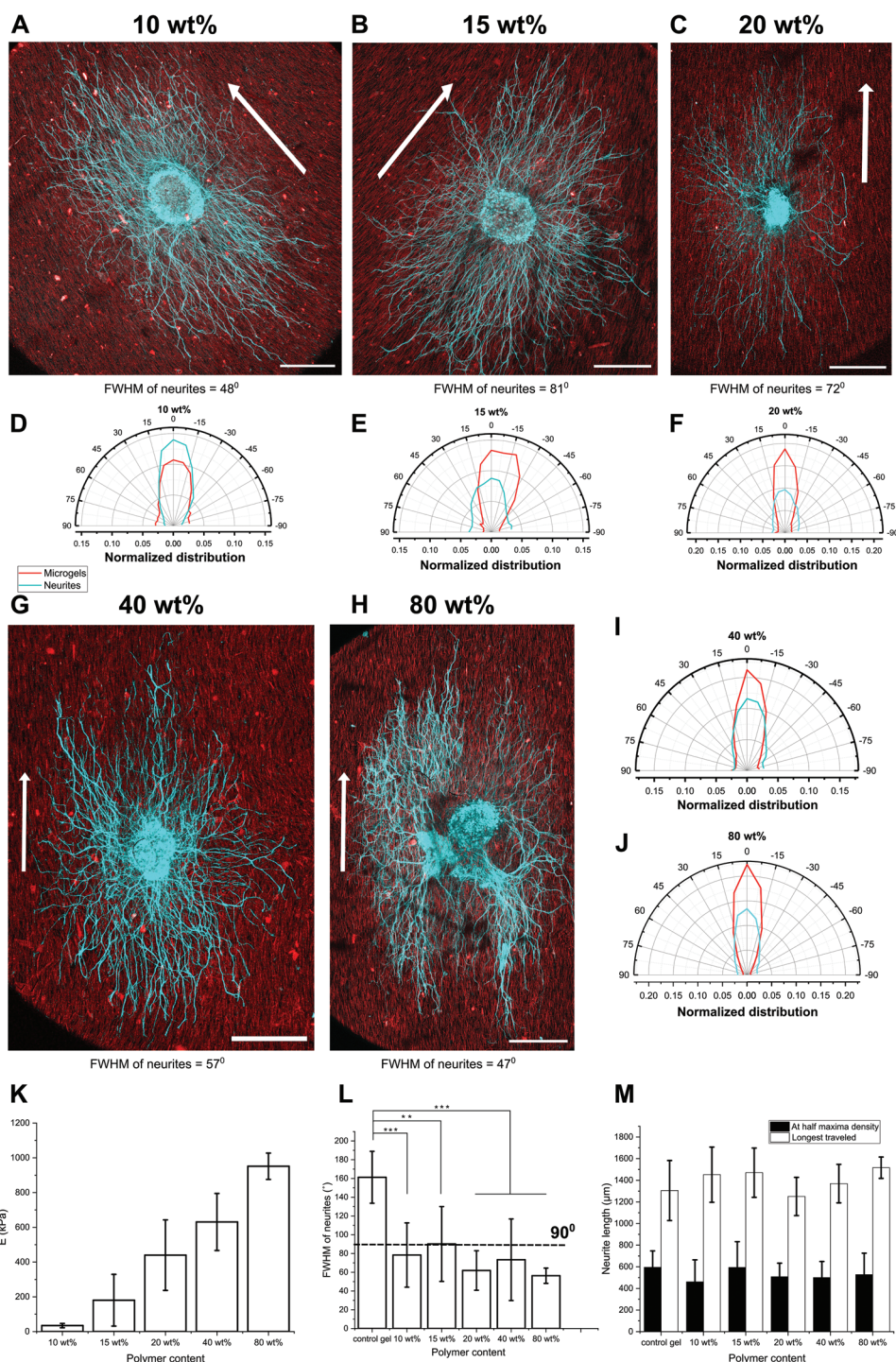
Figure 3. Comparison of neurite orientation and growth in Anisogels containing aligned microgels of different stiffness with dimensions of $2.5 \times 2.5 \times 50$ µm at 1 vol%. Confocal micrographs of neurites growing from DRGs after seven days of culture in Anisogels with microgels containing A) 10 wt.%, B) 15 wt.%, C) 20 wt.%, G) 40 wt.%, and H) 80 wt.% of PEG-DA with their corresponding normalized orientation distribution curves of neurites and microgels in figures (D–F) and (I, J). The white arrows indicate the direction of alignment of microgels. Cyan is b-tubulin and red is rhodamine-labeled microgels. Scale bar = 500 µm. n ≥ 3 in all conditions. K) Stiffness comparison plots of different microgel conditions measured using AFM point force spectroscopy. Comparison of neurite orientation and outgrowth between different microgel conditions are plotted in graphs (L) and (M) respectively. Data is presented as mean ± s.d. and statistical significance is performed using one-way ANOVA with Tukey comparison (* $p < 0.05$; ** $p < 0.01$; *** $p < 0.001$).

ADVANCED
SCIENCE NEWS
www.advancedsciencenews.com

ADVANCED
FUNCTIONAL
MATERIALS
www.afm-journal.de

a family of motor proteins called myosin, forming actomyosin complexes. The contractility of these actomyosin complexes upon cellular interaction with various cell adhesive ligands leads to an altered gene and protein expression, which further dictates the cell morphology, migration, and tissue morphogenesis.[51,60] So far in the case of PEG-based Anisogels, fibronectin is mixed and embedded inside the surrounding matrix to enable cell adhesion and promote neurite extension, while the microgels are bioinert and do not contain any cell adhesion sites.[35] In a previous publication, GRGDS modified microgels were used to study whether this would enhance neurite growth and alignment in both fibrin and PEG-based Anisogels. However, in neither of these cases, the biomodified microgels changed neurite growth.[40] We assumed that this might be because GRGDS is a generic cell adhesive peptide and might not be specific enough to promote neurites. Hence, in this report, we have mixed different long chain ECM biomolecules that are found in the central nervous system, such as fibronectin, laminin and hyaluronic acid, within the microgel precursor solution before crosslinking during PRINT.

Fibronectin (FN) is a commonly found glycoprotein in the ECM, which can support cell adhesion, migration and proliferation due to its interaction with cells, growth factors and several other ECM proteins.[61,62] It is a long chain dimer with a molecular weight of 440 kDa and has several binding domains for the attachment of cell integrins and ECM components like collagens and proteoglycans. Laminins (LN) are a major constituent of basal laminae and support the assembly of basement membrane found around Schwann cells. They promote cell adhesion and directional growth and migration of neurons, especially in the early stages of tissue development.[63,64] Hyaluronic acid or hyaluronan (HA) is a polysaccharide, which is a major component of the central nervous system ECM that binds other glycoproteins and proteoglycans, including ECM proteins like tenascins.[63,65] They are known to bind to specific cell surface receptors, actively promote cell proliferation, nerve regeneration and regulate inflammation.[20,66,67] In this study, the microgels are bio-functionalized by the addition of these molecules into the PEG precursor solution containing SPIONs, immediately after all the sonication steps, but before microgel cross-linking. The molecules are combined with the PEG precursor by gentle mixing to preserve the integrity of all the molecules, followed by the continuation of PRINT process as described in the Experimental Section. Each of these biomolecules are incorporated in such a way that their final concentration inside the microgels are 1 μm for FN, 100 μg mL^{-1} for LN and 2 mg mL^{-1} for HA. These concentrations are chosen based on the values previously reported in literature and from the limitations imposed by the microgel precursor composition such that only a small portion of the polymeric diluent gets replaced by the aqueous solutions of these biomolecules to avoid solvent evaporation during PRINT.[35,68,69] To confirm the incorporation of these biomolecules in microgels, an immunohistochemical staining is performed on them using corresponding antibodies. Figure S3 (Supporting Information) shows the fluorescent images of these microgels, with the biomodified ones displaying immunofluorescence when coupled with

anti-fibronectin, anti-laminin, and biotinylated hyaluronic acid binding protein respectively. All microgels are again 2.5 × 2.5 × 50 μm in dimensions, added at a 1 vol% concentration, and contain 400 μg mL^{-1} of SPIONs. In all cases except one, the surrounding matrix gel is modified with the addition of 1 μm fibronectin. In one condition, fibronectin in the matrix is replaced by laminin at a concentration of 50 μg mL^{-1} and combined with HA microgels to examine whether a combination of different biomolecules could be beneficial for the growth of neurons. The laminin concentration was chosen after following previous publications,[69] while at the same time maintaining the PEG concentration.

Interestingly, the results from the neurite orientation analysis from chick DRGs (**Figure 4**) show a common trend that the FWHM increases in the presence of bio-modified microgels. Only in case of FN modified microgels in an FN containing PEG matrix, that there is no significant difference in alignment compared to the unmodified microgels in an FN containing PEG matrix. However, the former condition has an average FWHM of 98 ± 49⁰ (thus above 90˚) compared to 65 ± 21˚ for the inert microgels. In comparison with the non-modified bioinert microgels, neurite orientation seems to be adversely affected by the availability of cell adhesion sites on the surface of the microgels. We hypothesize that cells might be overstimulated by the presence of these additional signaling molecules and that competition between the mechanical anisotropy imposed by the stiffer microgels and cellular signaling by the cell binding sites on the microgels might be detrimental to the maintenance of aligned growth in neurites. This observation is contradictory to many previous reports where the introduction of cell binding sites on guiding elements enhanced neurite alignment in the direction of aligned structures like polymer nanofibers.[70] However, it has also been reported elsewhere that as the spacing between nanofibers is increased, neurites were found to cross-over the fibers and spread in different directions as they preferred to make more cell-cell contacts than fiber-cell interactions.[71] In this report, nerves grow in between discrete, aligned micro-structures inside a 3D hydrogel, which is unique for our Anisogel platform. Here, enhancing the bioactivity and cell adhesiveness of the microgels is observed to be counteracting the physical and mechanical alignment function of the microgels, hypothetically due to the bio-attraction of microgels perpendicular to their long axis. In contrast, all the biomodified microgel conditions improve either one or both of the neurite growth parameters, the length at half maxima density and longest distance travelled. Both HA and LN microgels in fibronectin modified matrices cause a slight increase in neurite growth, whereas FN modified microgels significantly contribute to the elongation of neurites. The combination of HA microgels in laminin modified matrices is the most effective in enhancing both the density of growth and elongation of neurites. These findings are in agreement with previous reports on enhancement of neural progenitor stem cell survival, migration and differentiation in hydrogels containing a combination of hyaluronic acid and laminin molecules.[72,73] It could also be interesting to study a whole different combination of biomolecules in the future with this system.
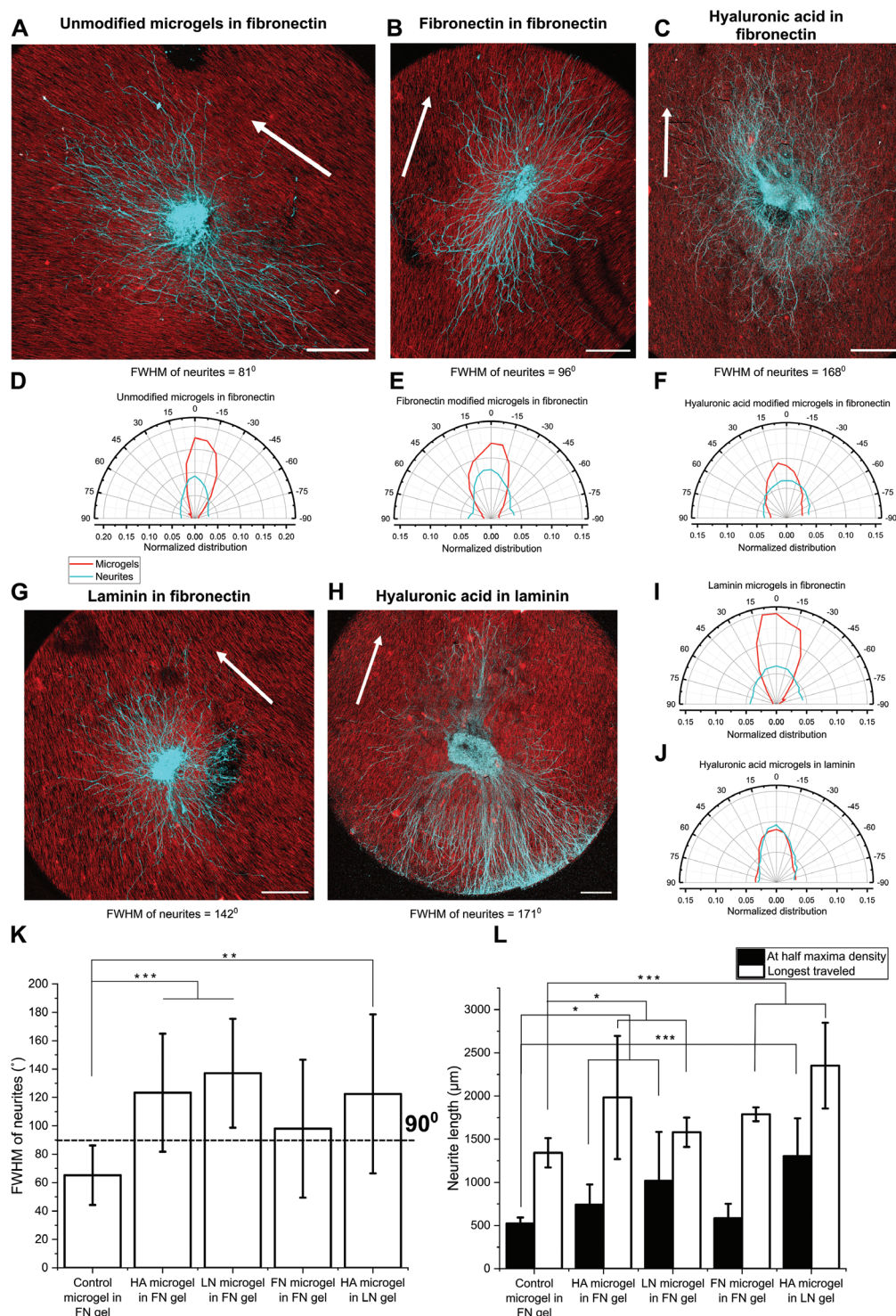
Figure 4. Comparison of neurite orientation and growth in Anisogels containing aligned microgels modified with different ECM molecules. Confocal micrographs of neurites growing from DRGs after seven days of culture in Anisogels with A) unmodified microgels, B) fibronectin modified microgels, C) hyaluronic acid modified microgels, G) laminin modified microgels in PEG matrices functionalized with fibronectin, and H) hyaluronic acid modified microgels in PEG matrix modified with laminin. The corresponding normalized orientation distribution curves of neurites and microgels are shown in figures (D–F) and (I, J). Cyan is b-tubulin and red is rhodamine-labeled microgels. Scale bar = 500 μm. $n \geq 3$ in all conditions. The white arrows indicate the direction of alignment of microgels. Comparison of neurite orientation and outgrowth between different microgel conditions are plotted in graphs (K) and (L) respectively. Data is presented as mean ± s.d. and statistical significance is performed using one-way ANOVA with Tukey comparison (* $p < 0.05$; ** $p < 0.01$; *** $p < 0.001$).

**ADVANCED
SCIENCE NEWS**
www.advancedsciencenews.com

**ADVANCED
FUNCTIONAL
MATERIALS**
www.afm-journal.de

2.4. Effect of Microgel Coupling to Matrix Gel

In most of the microgel-in-gel biphasic systems, microgels are just embedded inside a matrix hydrogel without a covalent coupling[74] and the same holds true in case of Anisogels, where all aligned microgel rods are simply encapsulated in the surrounding matrix.[74] This when combined with the fact that these microgels were mostly not cell-adhesive kept the cell interactions with microgels to the minimum in such systems. The microgels are able to induce neurite alignment primarily because of their relatively higher stiffness compared to the surrounding gel, making them function mostly as a barrier to guide the cells in a particular direction. Since cell elongation and proliferation in 3D matrices are significantly affected by the interactions of cells with the matrices through the actomyosin contractility as described before, we next investigated whether we can enhance this mechanobiological effect when microgels are covalently coupled to the PEG matrix and whether this would give rise to an altered cell response. As cells screen their 3D environment by pulling on their surrounding matrix, a connection between the surrounding hydrogel and the microgels may increase the effect of sensing the mechanical anisotropy of the Anisogel. When cells pull onto the matrix, which now is connected to the stiff microgels, a force transmission of different magnitude to the cells as well as a different viscoelastic response from the matrix is expected, as compared to the scenario where microgels are not coupled to the matrix. This covalent coupling is implemented by the modification of microgels with FXIIIa substrate peptides Q and K, which are used to cross-link the surrounding hydrogel. The peptides are coupled to the microgel surfaces post-PRINT production via a Michael-type addition reaction between the thiol groups of the cysteine-containing Q- and K-peptides and free remaining acrylate groups on the microgels. During the formation of the Anisogel, these peptides on the microgels can react enzymatically with the surrounding PEG precursor in the presence of FXIIIa.

The binding of Q and K peptides to the microgels are confirmed by performing a fluorescamine assay. No signals were observed for both unmodified microgels and microgels, which were reacted with these peptides in water where the Michael-type addition reaction cannot take place (Figure S4, Supporting Information). Thereafter, Anisogel samples were made with either the Q or K post-functionalized microgels in fibronectin modified PEG gels similar to the above cases. At first, the FWHM of microgel orientation was compared to see if the reaction between the peptides on microgels and the surrounding matrix would interfere with the hydrogel formation and microgel alignment. As can be seen from the graph and microgel images (**Figure 5**), at a concentration of 1 vol%, the $2.5 \times 2.5 \times 50$ µm sized microgels do align well in Anisogels with no significant difference in their FWHM from the control conditions with unreactive microgels. The neurite growth and orientation analysis, however, does not demonstrate any improvement by covalently coupling the microgels to the surrounding gel. Thus, the sensitivity of cells to mechanical anisotropy of the Anisogel is not increased by such modifications. In both the conditions of Q and K peptide modified microgels, the covalent coupling of microgels even impaired neurite alignment. The length of neurite outgrowth remains unchanged for the K microgels, while this is also reduced for the Q microgels in comparison with the condition where the microgels are simply aligned and embedded inside the PEG matrix.

To investigate the reason behind this observation, the mechanical properties of various Anisogel formulations are characterized. Macro-rheology on a rotational rheometer was first used as method to measure the storage modulus of different Anisogel samples. The graph in Figure S5 (Supporting Information) is obtained using 5 vol% of microgels instead of 1 vol%, to pick up on the differences in storage moduli more clearly. However, even at these microgels concentrations, the moduli are similar for all conditions except for the Anisogels with Q microgels. It is clear from these results that due to the shear forces employed in rheology, the readout is mainly determined by the surrounding gel and is less sensitive to the presence of the incorporated microgels. Therefore, we employed nanoindentation to measure the elastic modulus of these different Anisogel samples containing 1 vol% of $2.5 \times 2.5 \times 50$ µm microgels, which reveals that the overall stiffness of the Anisogels (both Q and K) is lowered when the microgels are covalently coupled to the matrix (Figure 5J). This can be explained as several functional arms of the star PEG conjugates in the precursor solution of the surrounding gel now take part in creating a chemical bond with the functionalized microgels as the same cross-linking chemistry is used for both reactions.

Although it has been shown by several groups that softer 3D hydrogel matrices are more suitable for nerve growth,[75,76] our surrounding gel was already extremely soft with an elastic modulus of 414 ± 209 Pa (measured by nanoindentation). Based on the available literature, we hypothesize that after microgel coupling, the network structure of the PEG hydrogel might be too loose for the growth cones of extending nerve cells to form stable adhesions for migration.[47] The current knowledge of correlation between substrate stiffness and cell spreading is centered on the formation of integrin-mediated adhesion complexes between the cell and its substrate and the force sensing through actomyosin contractility.[77,78] The lowering of stiffness in the matrix following the microgel coupling might, therefore, lead to the formation of too weak adhesion complexes that are not stable enough to support cell migration, decreasing the overall neurite growth. In addition, the coupling of the microgels to the surrounding gel may alter the anisotropic force propagation, negatively influencing the mechanical signals that promote unidirectional nerve growth.

3. Conclusions

The Anisogel is an innovative platform that enables guided growth of neurons by the presence of oriented magneto-responsive microgels. Besides the function of these microgels to act as barriers in a hydrogel matrix to ensure an aligned growth of neurites, they can also be a useful tool in understanding the various mechanobiological mechanisms that are involved in supporting oriented cell growth. In this regard, we have investigated various aspects of microgel properties in a synthetic PEG-based Anisogel system, such as their dimensions and concentrations, stiffness, surface modifications, and interactions with their matrix. It was observed that microgels need a higher
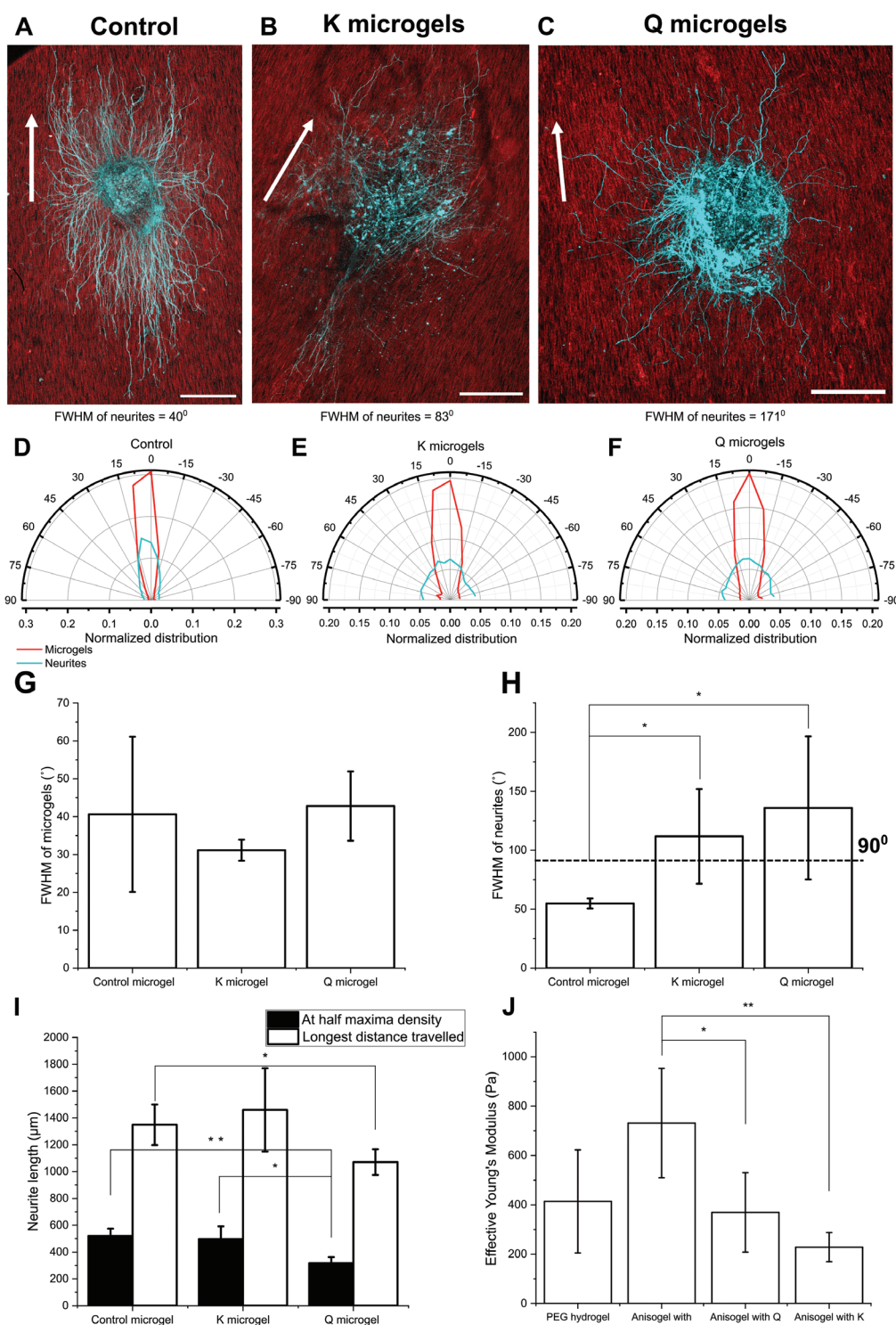
Figure 5. Comparison of neurite orientation and growth in Anisogels with the aligned microgels coupled to the matrix. Confocal micrographs of neurites growing from DRGs after seven days of culture in Anisogels with A) microgels encapsulated in the PEG matrix and microgels coupled with the PEG matrix after modification with B) K peptide and C) Q peptide along with their corresponding normalized orientation distribution curves of neurites and microgels in figures (D–F). The white arrows show the direction of the aligned microgels. Cyan is b-tubulin and red is rhodamine-labeled microgels. Scale bar = 500 μm. $n \geq 3$ in all conditions. Comparison of microgel and neurite orientation between different microgel conditions are plotted in graphs (G) and (H) respectively. The plot I) shows the neurite outgrowth measured as the length at half maxima density and maximum distance travelled. The nanoindentation stiffness of the PEG hydrogel or Anisogel samples are plotted in J). Data is presented as mean ± s.d. and statistical significance is performed using one-way ANOVA with Tukey comparison (* $p < 0.05$; ** $p < 0.01$; *** $p < 0.001$).

aspect ratio and be present in higher concentrations in PEG gels compared to fibrin gels to ensure sufficient neurite orientation, likely because the PEG gels are homogenous without any fibrous domains to provide additional guidance cues. Local changes in stiffness by altering the microgel stiffness did not produce any significant differences in neurite alignment or growth. However, the softest microgels used in this report still have a Young's modulus that is 100-fold higher than the surrounding hydrogel. Even softer rod-shaped microgels may in the future be produced by compartmentalized jet polymerization but then the dimensions would need to be further reduced to 2.5 µm diameter when using this new technique.[56] The use of specific ECM proteins to biomodify microgels resulted in an overall loss of alignment of neurites but promoted their growth and extension. This emphasizes that the directional guidance from the mechanical anisotropy imparted by the microgels is easily disturbed by the presence of local cell binding sites on these microgels. Thus, if an enhanced growth of neurites is desired while maintaining their orientation, it is important to ensure that the bioactive modifications provided are kept to a minimum and presented mainly in the surrounding matrix, in contrast to the microgels. Lastly, we investigated the effect of covalently coupling the microgels to the surrounding PEG matrix on neurite growth and orientation. This revealed that such a coupling results in a reduction of neurite alignment, as well as their growth, possibly due to an altered force propagation during cell growth. In future, it would be interesting to study whether an increase in microgel stiffness could compensate for the loss in neurite alignment due to the biomodification of the microgels. The microgels could also be modified with fibronectin binding domains, which could further orient the fibronectin in the matrix hydrogel during their magnetic alignment, which may further promote neurite orientation.

Besides the use of Anisogels as an in vitro tissue regenerative platform, they are also potential candidates for use as an injectable therapy to regenerate aligned tissues. Anisogels are being currently evaluated for their effectiveness in rat spinal cord injury models. Initial experiments in a spinal cord resection model in mouse cadavers showed that placing a stationary magnet close to the spinal cord, in a way that the magnetic field lines run parallel to the tissue, is sufficient to orient the magneto-responsive microgels and fix their orientation within the surrounding cross-linked hydrogel.[79] While this demonstrated a proof-of-principle of the injectability in vivo, we currently employ a variation of this setup, where an arrangement of magnets is positioned close to the spinal cord, with the field lines parallel to the tissue orientation during injection. After injection, the Anisogel is allowed to cross-link for ≈ 10–20 min, after which the magnets are removed. This approach can be easily adapted for its use in other aligned tissues.

4. Experimental Section

Production of Microgels: A silicon wafer with patterns corresponding to the required microgel dimensions was produced by photolithography (AMO GmbH) and fluorosilazined. A weighed quantity of polydimethylsiloxane (Sylgard 184, Sigma–Aldrich) mixed with the hardener in 1:10 ratio was cast over the wafer and cured for 4 h at 110 °C to produce a mould. A polymer precursor solution was prepared after several sonication steps containing different wt.% of PEG-DA (700 Da, Sigma–Aldrich), photoinitiator (Irgacure 2959, Sigma–Aldrich), and methacryloxyethyl thiocarbamoyl rhodamine B (Polysciences), diluent PEG-OH (200 Da, Sigma–Aldrich) and SPIONs (EMG-700, Ferrotec). For the biomodified microgels, solutions of fibronectin (Sigma–Aldrich), laminin (Sigma–Aldrich) or Hyaluronic acid (Advanced BioMatrix) were added to this precursor solution and mixed gently. The solution was spread thoroughly over the PDMS mould with the help of a polyethylene terephthalate (PET) foil (Goodfellow), laminated above the liquid layer. The foil was then carefully removed avoiding any bubble entrapment, to took away all the excess precursor solution. This mould was placed under a UV-light for 60 min in a nitrogen atmosphere for the polymer to cross-link. Thereafter, the mould was glued to a layer of 50% polyvinylpyrrolidone (360 kDa, Sigma–Aldrich) in water. Once the glue dried, the mould was peeled off and the microgels were harvested by dissolving the glue in fresh water. These were further purified by washing several times in water, followed by UV-sterilization, disinfection in 70% ethanol, washing in twice in sterile PBS (Lonza) and twice in cell culture medium (Dulbecco's Modified Eagle Medium (DMEM), (Lonza) supplemented with fetal bovine serum (Biowest) and antibiotic antimycotic (Gibco)). The final microgel suspension in cell culture medium was then counted using a Neubauer chamber and stored until use in 4 °C.

To prepare the Q and K peptide modified microgels, 2.7 mg of the Q peptide (2 µmol) and 3.4 mg of K peptide (2 µmol) were dissolved separately in 2 mL of a phosphate buffer (pH = 8) at a concentration of 1 м. Thereafter, the purified microgels, prepared as described previously, were re-dispersed in the Q/K peptide solution by a centrifugation followed by supernatant removal step. The solution was then gently stirred for 30 min for the Michael-type addition reaction to happen between the cysteine groups of the peptides and the acrylates on the microgels. After the conjugation, the microgels were washed twice in the phosphate buffer for 30 min to remove the unreacted peptides. Thereafter, the sterilization process, as mentioned previously was continued.

Matrix Hydrogel Preparation: The PEG hydrogel was prepared as described previously.[35,80] Briefly, two separate batches of 8 arm star PEG-vinylsulfone (sPEG-VS, 20 kDa, Jenkem Technology) were conjugated with different peptide solutions in triethanolamine (pH = 8, Sigma–Aldrich): (H-NQEQVSPLERCG-NH2: Q-peptide) (1358.6 Da, Pepscan) or (Ac-FKGGGPQGIWGQERCG-NH2: K-peptide) (1717.6 Da, Pepscan) using a Michael-type addition reaction via the thiol containing cysteine by incubating the solutions for 2 h at 37 °C. These solutions were then dialyzed for four days against water at 4 °C to remove any unreacted peptides. Following this, the solutions were lyophilized, dissolved in water, sterilized and stored at −20 °C until further use. For making the gels, the two PEG conjugates were mixed in an equimolar composition at a total of 1 wt.% in cell culture media, along with a 10X calcium buffer (0.1 м CaCl2, 0.5 м Tris, 1.1 м NaCl) and cell adhesive peptides: fibronectin (Sigma Aldrich) or laminin from mouse Engelbreth-Holm-Swarm sarcoma (Sigma Aldrich). The gelation was initiated by the addition of FXIII. For activating the enzyme FXIII (CSL Behring GmbH, 1250 U FXIII), a 200 U mL^{-1} thrombin (Sigma–Aldrich) solution is diluted to 20 U mL^{-1} in a buffer (25 м CaCl2, 10 mм TRIS, 150 mм NaCl) and was incubated with the FXIII for 30 min at 37 °C, while shaking gently every 5 min. The FXIIIa was then aliquoted and stored at −80 °C until further use.

Anisogel Preparation: To prepare the Anisogel samples, a calculated number of microgels were dispersed in a predetermined volume of DMEM medium by centrifugation and removal of supernatant. The rest of the components to prepare the PEG gels as mentioned above were added to this microgel suspension. After a thorough mixing immediately following the addition of FXIIIa, the solution was pipetted into a suitable chamber (Ibidi) with magnets fitted around them. DRGs for cell culture were obtained after the dissection of a 10 days old chicken embryo, which were then placed inside the pipetted precursor solutions. The samples were cross-linked for 30 min at 37 °C with the chambers flipped back and forth once in between to prevent settling of DRGs to the bottom

of the chamber. After the gelation was completed, cell culture media supplemented with nerve growth factor (PeproTech) at a concentration of 20 ng mL^{-1} was added to the samples and the DRGs were cultured for seven days with a media exchange done after every two days.

Calculation of Inter-Microgel Distance: The total number of microgels (*N*) that were required to achieve a certain concentration (vol%) in the Anisogel is calculated as follows:

$$N = \frac{vol\% \times V}{\nu} \qquad (1)$$

where *V* is the total volume of Anisogel to be prepared and ν is the volume of a single microgel rod calculated by multiplying its length (*l*), breadth (*b*) and thickness (*t*).

It is assumed that these microgels were homogeneously distributed throughout the Anisogel and that they were equidistant from each other both laterally and longitudinally, consider an Anisogel to be made of several cuboids with a microgel placed at one of its edges. The cuboid volume would then be the free volume (V_f) available for each microgel, which can be calculated using the equation below:

$$V_f = \frac{V}{N} \qquad (2)$$

Since this free volume is also equivalent to the volume of the cuboid, it can solve the following equation to calculate the inter-microgel distance (*d*).

$$V_f = (l+d) \times (b+d) \times (t+d) \qquad (3)$$

Immunofluorescent Staining and Imaging: After seven days of culture, the cell culture media was removed from the Anisogel samples, followed by washing with PBS for three times, 30 min each and then fixing with 4% paraformaldehyde solution (AppliChem) for 1 h with gentle shaking at 25 rpm at room temperature. After washing again thrice with PBS, the samples were incubated with 0.1% Triton X-100 (Sigma–Aldrich) solution in PBS for 30 min for permeabilization. Thereafter, the cells were blocked by incubating with 4% bovine serum albumin (BSA) (Sigma–Aldrich) solution in PBS for 4 h. This was followed by incubation with the primary antibody against Tubulin β3 (Biolegend, 1:250) in 4% BSA solution overnight at 4 °C. After washing thrice with PBS again, the samples were incubated with a secondary antibody, Alexa Fluor 633 goat anti-mouse (Invitrogen, 1:1000) in PBS for 4 h at room temperature. The samples were washed thrice once again with PBS to remove the secondary antibody and stored in PBS at 4 °C. The samples were imaged using a Leica SP8 Tandem Confocal microscope using an air objective of 10×/0.3 N.A. Z-stacks of 200 µm thickness are obtained for each sample. These images were captured using several excitation wavelengths and the emission signals were captured using suitable detectors (hybrid detectors or photomultipliers).

To confirm the presence of different biomolecules in microgels for section 2.3, several primary antibodies that specifically bind to fibronectin, laminin or hyaluronic acid are used. After the microgels were harvested and purified, they were incubated in 4% BSA solution in PBS for 4 h with gentle shaking. Thereafter, microgels were incubated with either anti-fibronectin (Abcam, 1:100), anti-laminin (Invitrogen, 1:100) or biotinylated hyaluronic acid binding protein (Merck, 5 µg mL^{-1}) solutions in 4% BSA solution for ≈16 h. After this, the primary antibody solutions were exchanged with fresh PBS thrice and the microgels were incubated with secondary antibody solutions in PBS for 4 h with gentle shaking. Alexa Flour 633 goat anti-rabbit (Invitrogen, 1:1000) antibody was used for the control, fibronectin, and laminin modified microgels. Streptavidin conjugated Alexa Flour 633 (Invitrogen, 1:1000) antibody was used for the Hyaluronic acid modified microgels. The control microgels were not exposed to any primary antibodies and were directly stained with Alexa Flour 633 goat anti-rabbit (Invitrogen, 1:1000) to confirm there was no auto-fluorescence from the microgels or a cross talk from the Rhodamine dye.

Analysis of Neurite Alignment and Radial Growth: The first five slices (≈21 µm) from the z-stacks were first cropped out to remove the signals close to the bottom of the chamber. The resultant z-stack images were then processed using Fiji Image J to give a maximum intensity projection and a mask was drawn manually around the explant/core of the DRG to remove it from the image. All images of the mask, microgels, and DRGs were grouped separately and the analysis was performed blindly via a python code. In order to extract the orientation of structures from these images, a highly elliptic "Mexican hat" filter rotated to 20 angle values between 0 and 180 degrees is applied as reported previously.[35] Images were first background corrected and for this, the convolution of a normalized Gaussian kernel (width 10 pixels, window size 81 pixels) of the image was calculated, and the resulted blurred image was subtracted as background. Negative pixel values were set to zero. Then structures were smoothed again applying a convolution filter using a normalized Gaussian kernel, this time with a width of 0.5, 1.0 or 1.5 pixels (depending on the image stack) and 11 pixels window size. In cases when the dynamic range of the image stack was high, the range was compressed applying a ½ power law (square root) to the intensity values before further processing and then the structures were smoothed again applying a convolution filter using a normalized Gaussian kernel. The applied "Mexican hat" filter had a width of 10 pixels along its long axis and 1 pixel along its short axis. The window size was 61 pixels in both directions. The kernel was the second derivative of a Gaussian in both directions. Resulted images were collected as a 3D stack, where the z-axis decodes the orientation angles. A maximum projection was applied along the z-axis to identify the local maxima, and then the corresponding angle was identified for each pixel (angle image). A threshold (using Otsu's method) was applied to the collected maximum intensities (after removing the pixels corresponding to the explant by applying the mask), to identify pixels that belong to objects versus those which were background. Orientation histograms were calculated from the angle values of object pixels only and the FWHM from these histograms were used as a measure of neurite alignment. Only those samples had their FWHM values below 90˚ were considered as aligned.

For the neurite outgrowth analysis, images were again background corrected the same way as described for orientation analysis. The background blur was calculated with a normalized Gaussian kernel with a width of 10 pixels and window width of 81 pixels. The smoothing filter had a width of 1.5 pixels and window size of 11 pixels. The dynamic range of the image was compressed applying a square-root to the intensity of the images. Pixels belonging to the cells were determined using the dynamic threshold calculated by the method of Otsu.[81] Center of the structure was determined using the center of the explant provided as a mask. All pixels of the cells were converted to radial coordinates around this center. Distances were determined as the radius from the center. Histograms of distance were then calculated for each pixels in the image. The neurite length at half maxima density and the longest distance travelled were calculated from these histograms as reported previously.[44] Neurite growth at half-maximum density was defined as the distance between the edge of the explant and the distance at which the neurite density approaches a half-maximum value. The longest distance travelled by neurites was defined as the distance from the edge of the explant until the pixel density drops to < 0.001 pixels per µm^2.

Statistical Analysis: Statistical analysis of the data was conducted in OriginPro 2020 using a one-way ANOVA. Pair comparisons were performed using Tukey's methods, where *p*-value below 0.05 was considered as a significant difference (*$p < 0.05$; **$p < 0.01$; ***$p < 0.001$).

Stiffness Measurement of Microgels and Analysis by AFM: AFM point force spectroscopy was performed using a Dimension Icon AFM (Bruker) using a colloidal probe CP-PNPL-PS-D-5 (Nano and more) with a diameter of ≈ 2 µm. Force curves are measured with an approach and retraction speed set to 1 µm s^{-1}, with a waiting time of 100 ms at contact. The maximal relative force was set to 4 nN. All curves were exported to ASCII files with the analysis software of the instrument. The approach part of the curves was analyzed using a home written script in Python [https://www.python.org] using the Hertz model (equation (1)). The Poisson ratio was assumed to be that of an incompressible material

($\nu = 0.5$). The last 20% of the data points were fitted to a line and subtracted as background.

$$F(\delta) = \frac{4}{3}\frac{E}{1-\nu^2}\sqrt{R}(\delta - \delta_0)^{3/2} \qquad (4)$$

The model was fit up to 5 nN force, practically the whole force range of the curve using a nonlinear fit (leastsq() from Scipy [https://www.scipy.org]) finding both the Young's modulus and the contact point. Atleast three microgels were intended per condition and an average of all the indentations per microgel was calculated as its stiffness.

Rheological Characterization: The rheological characterization of the PEG gels and Anisogels were performed on a DHR 3 Rheometer from TA instruments at 37 °C using a cone plate geometry, with a 2° cone angle and at 51 µm truncation gap. The time sweep measurements were recorded at 0.5 Hz frequency and 2% strain for 30min until the storage modulus curve reaches a plateau. The point at which the tan (δ) value drops below 0.1 was taken as the point of gelation and storage modulus was taken as the average of all values after this time point.

Fluorescamine Assay: The coupling of Q and K peptides to the microgel surfaces were confirmed by a fluorescamine assay (Sigma) that was used to detect the presence of primary amines. 30 µL of a fluorescamine solution in acetone (0.3 mg mL^{-1}) was mixed with 90 µL of Q/K-microgel suspension and examined by fluorescence spectroscopy using a 365 nm light. As negative controls, microgels without any peptide functionalization were prepared and examined using the same procedure.

Nanoindentation of Anisogels to Measure their Elastic Modulus: A 10 µL gel droplet of each Anisogel condition was made on a well plate and were analyzed for their elastic moduli using a nanoindentor called Chiaro (Optics11Life, Amsterdam, The Netherlands). Three samples per condition were tested with a minimum of ten indentations on different locations on each droplet. Indentation measurements were performed using a cantilever-based probe with a spherical tip radius of 22.5 µm and a cantilever stiffness of 0.3 N m^{-1}. The indentation-depth is 5 µm. From the obtained load–indentation curves, a Hertz contact model was used to calculate the effective Young´s modulus E (kPa). All measurements were performed at room temperature.

Supporting Information

Supporting Information is available from the Wiley Online Library or from the author.

Acknowledgements

Conflict of Interest

The authors declare no conflict of interest.

Data Availability Statement

The data that support the findings of this study are available from the corresponding author upon reasonable request.

[1] R. Sakaguchi, J. Ferracane, *Craig's Restorative Dental Materials*, 14th ed., **2019**, pp. 313–326, https://doi.org/10.1016/B978-0-323-47821-2.00016-0.

[2] J. A. Baddour, K. Sousounis, P. A. Tsonis, *Birth Defects Res. Part C Embryo Today Rev.* **2012**, *96*, 1.

[3] A. K. Gaharwar, I. Singh, A. Khademhosseini, *Nat. Rev. Mater.* **2020**, *5*, 686.

[4] A. S. Mao, D. J. Mooney, *Proc. Natl. Acad. Sci. USA* **2015**, *112*, 14452.

[5] P. Y. W. Dankers, J. M. Boomker, E. W. Meijer, E. R. Popa, M. J. A. van Luyn, *J. Controlled Release* **2011**, *152*, 177.

[6] B. V. Slaughter, S. S. Khurshid, O. Z. Fisher, A. Khademhosseini, N. A. Peppas, *Adv. Mater.* **2009**, *21*, 3307.

[7] J. A. Hunt, R. Chen, T. van Veen, N. Bryan, *J. Mater. Chem. B* **2014**, *2*, 5319.

[8] J. Gerardo-Nava, T. Führmann, K. Klinkhammer, N. Seiler, J. Mey, D. Klee, M. Möller, P. D. Dalton, G. A. Brook, *Nanomedicine* **2008**, *4*, 11.

[9] A. Kriebel, M. Rumman, M. Scheld, D. Hodde, G. Brook, J. Mey, *J. Biomed. Mater. Res., Part B* **2014**, *102*, 356.

[10] N. Park, J. Kim, *ACS Appl. Mater. Interfaces* **2022**, *14*, 4479.

[11] C. J. Lowe, I. M. Reucroft, M. C. Grota, D. I. Shreiber, *ACS Biomater. Sci. Eng.* **2016**, *2*, 643.

[12] L. H. Nguyen, M. Gao, J. Lin, W. Wu, J. Wang, S. Y. Chew, *Sci. Rep.* **2017**, *7*, 42212.

[13] S. Yang, J. Zhu, C. Lu, Y. Chai, Z. Cao, J. Lu, Z. Zhang, H. Zhao, Y.-Y. Huang, S. Yao, X. Kong, P. Zhang, X. Wang, *Bioact. Mater.* **2022**, *8*, 529.

[14] A. Hurtado, J. M. Cregg, H. B. Wang, D. F. Wendell, M. Oudega, R. J. Gilbert, J. W. McDonald, *Biomaterials* **2011**, *32*, 6068.

[15] J. Li, C. Wu, P. K. Chu, M. Gelinsky, *Mater. Sci. Eng. R Reports* **2020**, *140*, 100543.

[16] C. Li, M. Kuss, Y. Kong, F. Nie, X. Liu, B. Liu, A. Dunaevsky, P. Fayad, B. Duan, X. Li, *ACS Biomater. Sci. Eng.* **2021**, *7*, 690.

[17] B. Kessel, M. Lee, A. Bonato, Y. Tinguely, E. Tosoratti, M. Zenobi-Wong, *Adv. Sci.* **2020**, *7*, 2001419.

[18] J.-A. Yang, J. Yeom, B. W. Hwang, A. S. Hoffman, S. K. Hahn, *Prog. Polym. Sci.* **2014**, *39*, 1973.

[19] S. Babu, F. Albertino, A. Omidinia Anarkoli, L. De Laporte, *Adv. Healthcare Mater.* **2021**, *10*, 2002221.

[20] J. K. Mouw, G. Ou, V. M. Weaver, *Nat. Rev. Mol. Cell Biol.* **2014**, *15*, 771.

[21] A. Jagiełło, Q. Hu, U. Castillo, E. Botvinick, *Acta Biomater.* **2021**, *141*, 39.

[22] S. Zhang, M. A. Greenfield, A. Mata, L. C. Palmer, R. Bitton, J. R. Mantei, C. Aparicio, M. O. de la Cruz, S. I. Stupp, *Nat. Mater.* **2010**, *9*, 594.

[23] E. J. Berns, S. Sur, L. Pan, J. E. Goldberger, S. Suresh, S. Zhang, J. A. Kessler, S. I. Stupp, *Biomaterials* **2014**, *35*, 185.

[24] Z. Álvarez, A. N. Kolberg-Edelbrock, I. R. Sasselli, J. A. Ortega, R. Qiu, Z. Syrgiannis, P. A. Mirau, F. Chen, S. M. Chin, S. Weigand, E. Kiskinis, S. I. Stupp, *Science (80-.)*. **2021**, *374*, 848.

[25] D. Ceballos, X. Navarro, N. Dubey, G. Wendelschafer-Crabb, W. R. Kennedy, R. T. Tranquillo, *Exp. Neurol.* **1999**, *158*, 290.

[26] N. Dubey, P. C. Letourneau, R. T. Tranquillo, *Biomaterials* **2001**, *22*, 1065.

[27] K. J. De France, K. G. Yager, K. J. W. Chan, B. Corbett, E. D. Cranston, T. Hoare, *Nano Lett.* **2017**, *17*, 6487.

[28] K. J. De France, M. Badv, J. Dorogin, E. Siebers, V. Panchal, M. Babi, J. Moran-Mirabal, M. Lawlor, E. D. Cranston, T. Hoare, *ACS Biomater. Sci. Eng.* **2019**, *5*, 2235.

[29] M. Antman-Passig, O. Shefi, *Nano Lett.* **2016**, *16*, 2567.

[30] J. Kim, J. R. Staunton, K. Tanner, *Adv. Mater.* **2016**, *28*, 132.

[31] B. Ankamwar, T. C. Lai, J. H. Huang, R. S. Liu, M. Hsiao, C. H. Chen, Y. K. Hwu, *Nanotechnology* **2010**, *21*, 075102.

[32] J. C. Rose, M. Cámara-Torres, K. Rahimi, J. Köhler, M. Möller, L. De Laporte, *Nano Lett.* **2017**, *17*, 3782.

[33] A. Omidinia-Anarkoli, S. Boesveld, U. Tuvshindorj, J. C. Rose, T. Haraszti, L. De Laporte, *Small* **2017**, *13*, https://doi.org/10.1002/smll.201770191.

[34] A. Omidinia-Anarkoli, S. Boesveld, U. Tuvshindorj, J. C. Rose, T. Haraszti, L. De Laporte, *Small* **2017**, *13*, 1702207.

[35] C. Licht, J. C. Rose, A. O. Anarkoli, D. Blondel, M. Roccio, T. Haraszti, D. B. Gehlen, J. A. Hubbell, M. P. Lutolf, L. De Laporte, *Biomacromolecules* **2019**, *20*, 4075.

[36] H.-R. Lin, C.-J. Kuo, C. Y. Yang, S.-Y. Shaw, Y.-J. Wu, *J. Biomed. Mater. Res.* **2002**, *63*, 271.

[37] B. B. Crow, A. F. Borneman, D. L. Hawkins, G. M. Smith, K. D. Nelson, *Tissue Eng.* **2005**, *11*, 1077.

[38] T. Darestani Farahani, M. Abtahi, A. A. Entezami, H. Mobedi, *Iran. Polym. J.* **2005**, *14*, 753.

[39] A. D. Lynn, T. R. Kyriakides, S. J. Bryant, *J. Biomed. Mater. Res. Part A* **2010**, *93A*, 941.

[40] J. C. Rose, D. B. Gehlen, T. Haraszti, J. Köhler, C. J. Licht, L. De Laporte, *Biomaterials* **2018**, *163*, 128.

[41] S. Dupont, L. Morsut, M. Aragona, E. Enzo, S. Giulitti, M. Cordenonsi, F. Zanconato, J. Le Digabel, M. Forcato, S. Bicciato, N. Elvassore, S. Piccolo, *Nature* **2011**, *474*, 179.

[42] Y. Chandorkar, A. Castro Nava, S. Schweizerhof, M. Van Dongen, T. Haraszti, J. Köhler, H. Zhang, R. Windoffer, A. Mourran, M. Möller, L. De Laporte, *Nat. Commun.* **2019**, *10*, 4027.

[43] J. C. Rose, D. B. Gehlen, A. Omidinia-Anarkoli, M. Fölster, T. Haraszti, E. E. Jaekel, L. De Laporte, *Adv. Healthcare Mater.* **2020**, *9*, 2000886.

[44] S. Vedaraman, D. Bernhagen, T. Haraszti, C. Licht, A. Castro Nava, A. Omidinia Anarkoli, P. Timmerman, L. De Laporte, *Biomater. Sci.* **2021**, *9*, 4329.

[45] C. Wang, X. Tong, X. Jiang, F. Yang, *J. Biomed. Mater. Res. Part A* **2017**, *105*, 770.

[46] M. Ehrbar, A. Sala, P. Lienemann, A. Ranga, K. Mosiewicz, A. Bittermann, S. C. Rizzi, F. E. Weber, M. P. Lutolf, *Biophys. J.* **2011**, *100*, 284.

[47] A. D. Doyle, N. Carvajal, A. Jin, K. Matsumoto, K. M. Yamada, *Nat. Commun.* **2015**, *6*, 8720.

[48] S. C. Rizzi, M. Ehrbar, S. Halstenberg, G. P. Raeber, H. G. Schmoekel, H. Hagenmüller, R. Müller, F. E. Weber, J. A. Hubbell, *Biomacromolecules* **2006**, *7*, 3019.

[49] M. Ehrbar, S. C. Rizzi, R. Hlushchuk, V. Djonov, A. H. Zisch, J. A. Hubbell, F. E. Weber, M. P. Lutolf, *Biomaterials* **2007**, *28*, 3856.

[50] J. P. Rolland, B. W. Maynor, L. E. Euliss, A. E. Exner, G. M. Denison, J. M. DeSimone, *J. Am. Chem. Soc.* **2005**, *127*, 10096.

[51] T. Iskratsch, H. Wolfenson, M. P. Sheetz, *Nat. Rev. Mol. Cell Biol.* **2014**, *15*, 825.

[52] R. J. Pelham, Y. Wang, *Proc. Natl. Acad. Sci. USA* **1997**, *94*, 13661.

[53] B. J. DuChez, A. D. Doyle, E. K. Dimitriadis, K. M. Yamada, *Biophys. J.* **2019**, *116*, 670.

[54] R. S. Stowers, S. C. Allen, L. J. Suggs, *Proc. Natl. Acad. Sci. USA* **2015**, *112*, 1953.

[55] M. Ehrbar, A. Sala, P. Lienemann, A. Ranga, K. Mosiewicz, A. Bittermann, S. C. Rizzi, F. E. Weber, M. P. Lutolf, *Biophys. J.* **2011**, *100*, 284.

[56] A. J. D. Krüger, O. Bakirman, L. P. B. Guerzoni, A. Jans, D. B. Gehlen, D. Rommel, T. Haraszti, A. J. C. Kuehne, L. De Laporte, *Adv. Mater.* **2019**, n/a, 1903668.

[57] A. J. D. Krüger, J. Köhler, S. Cichosz, J. C. Rose, D. B. Gehlen, T. Haraszti, M. Möller, L. De Laporte, *Chem. Commun.* **2018**, *54*, 6943.

[58] J. Dumbleton, P. Agarwal, H. Huang, N. Hogrebe, R. Han, K. J. Gooch, X. He, *Cell. Mol. Bioeng.* **2016**, *9*, 277.

[59] B. Alberts, A. Johnson, J. Lewis, M. Raff, K. Roberts, P. Walter, *Molecular Biology of the Cell*, Garland Science, New York **2002**.

[60] M. Murrell, P. W. Oakes, M. Lenz, M. L. Gardel, *Nat. Rev. Mol. Cell Biol.* **2015**, *16*, 486.

[61] M. M. T. Federico, M. Mayumi, T. Stephanie, B.-D. Dror, K. G. A. M. Ralph, L. Erella, S. A. Eming, J. A. Hubbell, *Sci. Transl. Med.* **2011**, *3*, 100ra89.

[62] M. M. Martino, J. A. Hubbell, *FASEB J. Off. Publ. Fed. Am. Soc. Exp. Biol.* **2010**, *24*, 4711.

[63] C. S. Barros, S. J. Franco, U. Müller, *Cold Spring Harb. Perspect. Biol.* **2011**, *3*, a005108.

[64] K. Ji, S. E. Tsirka, *J. Neuroinflammation* **2012**, *9*, 159.

[65] A. C. Bellail, S. B. Hunter, D. J. Brat, C. Tan, E. G. Van Meir, *Int. J. Biochem. Cell Biol.* **2004**, *36*, 1046.

[66] E. R. Burnside, E. J. Bradbury, *Neuropathol. Appl. Neurobiol.* **2014**, *40*, 26.

[67] S. K. Seidlits, Z. Z. Khaing, R. R. Petersen, J. D. Nickels, J. E. Vanscoy, J. B. Shear, C. E. Schmidt, *Biomaterials* **2010**, *31*, 3930.

[68] R. C. Gupta, R. Lall, A. Srivastava, A. Sinha, *Front. Vet. Sci.* **2019**, *6*, https://doi.org/10.3389/fvets.2019.00192.

[69] D. Barros, E. Conde-Sousa, A. M. Gonçalves, W. M. Han, A. J. García, I. F. Amaral, A. P. Pêgo, *Biomater. Sci.* **2019**, *7*, 5338.

[70] J. Xie, W. Liu, M. R. MacEwan, P. C. Bridgman, Y. Xia, *ACS Nano* **2014**, *8*, 1878.

[71] A. Omidinia-Anarkoli, J. W. Ephraim, R. Rimal, L. De Laporte, *Acta Biomater.* **2020**, https://doi.org/10.1016/j.actbio.2020.07.014.

[72] J. Arulmoli, H. J. Wright, D. T. T. Phan, U. Sheth, R. A. Que, G. A. Botten, M. Keating, E. L. Botvinick, M. M. Pathak, T. I. Zarembinski, D. S. Yanni, O. V. Razorenova, C. C. W. Hughes, L. A. Flanagan, *Acta Biomater.* **2016**, *43*, 122.

[73] C. P. Addington, J. M. Heffernan, C. S. Millar-Haskell, E. W. Tucker, R. W. Sirianni, S. E. Stabenfeldt, *Biomaterials* **2015**, *72*, 11.

[74] S. Kühn, J. Sievers, A. Stoppa, N. Träber, R. Zimmermann, P. B. Welzel, C. Werner, *Adv. Funct. Mater.* **2020**, *30*, 1908857.

[75] P. C. Georges, W. J. Miller, D. F. Meaney, E. S. Sawyer, P. A. Janmey, *Biophys. J.* **2006**, *90*, 3012.

[76] A. Banerjee, M. Arha, S. Choudhary, R. S. Ashton, S. R. Bhatia, D. V. Schaffer, R. S. Kane, *Biomaterials* **2009**, *30*, 4695.

[77] M. A. Wozniak, C. S. Chen, *Nat. Rev. Mol. Cell Biol.* **2009**, *10*, 34.

[78] D. E. Discher, P. Janmey, Y.-L. Wang, *Science (80-.)*. **2005**, *310*, 1139.

[79] J. C. Rose, M. Fölster, L. Kivilip, J. L. Gerardo-Nava, E. E. Jaekel, D. B. Gehlen, W. Rohlfs, L. De Laporte, *Polym. Chem.* **2020**, *11*, 496.

[80] M. Ehrbar, S. C. Rizzi, R. G. Schoenmakers, B. San Miguel, J. A. Hubbell, F. E. Weber, M. P. Lutolf, *Biomacromolecules* **2007**, *8*, 3000.

[81] N. Otsu, *IEEE Trans. Syst. Man. Cybern.* **1979**, *9*, 62.